Influence of Local Liquid Structure on Orientational Dynamics: Isotropic Phase of Liquid Crystals

John J. Stankus, Renato Torre,† and M. D. Fayer*

Department of Chemistry, Stanford University, Stanford, California 94305

Received: April 21, 1993; In Final Form: June 30, 1993®

Measurements of orientational relaxation over 6 decades in time (femtoseconds to nanoseconds) and 10 decades of amplitude are reported for the liquid crystal *N*-(methoxybenzylidene)butylaniline (MBBA) in its isotropic phase. The measurements were made using the transient grating optical Kerr effect method. The faster dynamics (picoseconds to nanoseconds) display a power law decay that is *temperature independent* up to 43 deg above the nematic–isotropic phase transition. The slower dynamics (tens of nanoseconds) obey the Landau–de Gennes (LdG) modified Debye–Stokes–Einstein hydrodynamic equation. The faster dynamics become temperature dependent at the same temperature that the slower dynamics begin to deviate from LdG behavior. The onset of temperature dependence and the deviation from LdG behavior occur when the size of the pseudonematic domain, defined in terms of the correlation length ξ, falls below $3\xi_0$. The temperature-independent dynamics is attributed to the local nematic structure, which exists on short time and distance scales. The temperature-independent orientational dynamics occur by relaxation of the local nematic structure back to a momentary minimum of the local free energy surface, rather than by diffusive orientational randomization. Two types of processes are discussed that can give rise to the power law decay: a parallel process (Förster direct transfer model) and a serial process (hierarchically constrained dynamics model). The MBBA experimental results are compared to earlier work on the liquid crystal pentylcyanobiphenyl. Remarkably, the same power law decay exponent (–0.63) and the same correlation length for the onset of deviation from LdG behavior ($\cong 3\xi_0$) are seen in both liquid crystals.

I. Introduction

Orientational relaxation is commonly discussed in terms of hydrodynamic theory.[1,2] A molecule is assumed to undergo orientational diffusion in a featureless continuous medium. The rate of orientational diffusion (decay of the orientational correlation function) is described by the Debye–Stokes–Einstein equation.[2,3] The orientational correlation function decay is exponential with a decay constant, τ, which is proportional to the molecular volume and viscosity and inversely proportional to the temperature. Since the viscosity usually decreases exponentially with increasing temperature, τ decreases rapidly as the temperature is raised.

The hydrodynamic continuum model does not consider anisotropic intermolecular interactions which can give rise to local structures in liquids. For example, it is known from neutron scattering that in both benzene and naphthalene neat liquids the molecules reside in crooked T-shaped structures.[4] These structures are not stable but exist on a time scale that is short compared to the time for rotational diffusion. Recent experiments have demonstrated that, in liquids having significant local structure, fast orientational relaxation can be unrelated to hydrodynamic motions.[5a,6-9] In fact, dynamics in a variety of types of systems are observed to be viscosity/temperature (η/T) independent over wide ranges of η/T. Experimental results[5a,6-8] have been explained in terms of a model that states the orientational relaxation dynamics arise from relaxation on the free energy potential surface that is responsible for the formation of the local structures rather than rotational diffusion. A perturbation, either optical or thermal, moves the system away from the local potential minimum. Then, the system relaxes back to the minimum, regenerating the original local structure. On a longer time scale, the system will undergo rotational diffusion which randomizes the local structure. However, on a time scale short compared to rotational diffusion, orientational relaxation is nonhydrodynamic and is decoupled from the bulk viscosity.

One liquid that exhibited this type of nonhydrodynamic behavior is the liquid crystal pentylcyanobiphenyl (5CB) in its isotropic phase. Here we report extensive studies of another liquid crystal, *N*-(methoxybenzylidene)butylaniline (MBBA). The experiments examine the orientational relaxation dynamics over 6 decades of time and 10 decades of signal decay using the transient grating optical Kerr effect (TG-OKE) experimental method. The similarities in behavior observed for MBBA and 5CB are striking and may suggest a universal orientational relaxation behavior of liquid crystals in their isotropic phase at both short and long times.

Just above the nematic–isotropic phase transition of a liquid crystal, the material is macroscopically a normal liquid, but it displays a variety of properties not common to simple liquids. These pretransitional effects are due to short-range molecular orientational order. The nematic–isotropic phase transition is weakly first order, and many properties of the isotropic liquid show critical behavior close to the transition temperature. The short-range order is characterized by a coherence or correlation length, $\xi(T)$. The temperature dependence of the correlation length was shown to be

$$\xi(T) = \xi_0\{T^*/(T - T^*)\}^{1/2}$$

by de Gennes' application of the Landau theory of second-order phase transitions to the weakly first-order transition in liquid crystals. ξ_0 is on the order of the molecular length, and T^* is a temperature slightly below the nematic–isotropic phase transition temperature, T_{ni}. Below T_{ni} the domain size becomes infinite.[10,11] Immediately above the phase transition, the correlation length is of the order of $20\xi_0$; the pseudonematic domains have "diameters" of the order 100–200 Å. Landau–de Gennes (LdG) theory applies to static parameters such as magnetic[12] and electric birefringence[13,14] and scattered light intensity[12,15] as well as dynamic effects seen in nuclear spin–lattice relaxations,[16,17]

† Permanent address: European Laboratory of Non-Linear Spectroscopy (LENS), University of Florence, Largo E. Fermi 2, Firenze, Italy.

® Abstract published in *Advance ACS Abstracts*, September 1, 1993.

0022-3654/93/2097-9478$04.00/0

dynamic light scattering (DLS),[12,15] and the optical Kerr effect (OKE)[14,18-21] in the temperature region just above the nematic–isotropic phase transition. Deviations from LdG theory have been seen in transient grating optical Kerr effect (TG-OKE) experiments[5] and in magnetic and electric birefringence[22] at temperatures sufficiently above the nematic–isotropic transition.

The local order in the isotropic phase of a liquid crystal is a consequence of the substantial anisotropy in the intermolecular interactions that gives rise to the nematic phase and still exists in the isotropic phase. The amount of local order can be characterized by a "local" order parameter, S_l,

$$S_l = {}^1/_2\langle 3\cos^2\theta - 1\rangle$$

where θ is relative to a direction, called the local director, that maximizes S_l.

In this paper we present an investigation of the effects this local liquid structure has on the molecular orientational dynamics of MBBA. Hydrodynamic theory has been successful in explaining behavior in simple liquids[2,23-25] and, with the modification from LdG theory, explains the slow dynamics in isotropic liquid crystals close to the phase transition. Here we report nonhydrodynamic molecular reorientational dynamics in MBBA of the same form as those we have seen in 5CB.[5a] The nonhydrodynamic orientational relaxation is associated with fast motions within the pseudonematic domains which remain viscosity/temperature independent over a broad viscosity/temperature range. The intradomain orientational dynamics occur over a wide range of times from picoseconds to nanoseconds. The motions within the domains are decoupled from the bulk viscosity of the liquid and are controlled by the local structure of the domains. The time dependence of the intradomain dynamics in both MBBA and 5CB is a power law decay. We present two models that can give rise to power law decays, a parallel process (Förster direct transfer model) or a serial process (hierarchically constrained dynamics model).

Early work on the dynamics of the isotropic phase of nematic liquid crystals focused on the slow hydrodynamic-like motion caused by order parameter fluctuations. These slow dynamics are well described by Landau–de Gennes theory and are the collective relaxation of the domain structure.[12,14,15,18-21,26,27] Flytzanis and Shen[28] pointed out that there should be additional orientational motions corresponding to fast motions within the pseudonematic domains. Fast effects were shown to exist by both time domain[29] and frequency domain[30] experiments. These experiments had limited time resolution or temperature range, which did not permit quantitative analysis of the data. Quantitative analysis of these effects was made possible by using TG-OKE experiments which increased the time resolution by 4 orders of magnitude over the bulk of previous experiments.[14,18,19-21] We have previously performed these higher-resolution TG-OKE experiments over a large temperature range on 5CB,[5a] and we have extended the measurements to MBBA in this paper.

Molecular dynamics can be probed by various spectroscopic techniques. These techniques include Raman spectroscopy, infrared line shape analysis, neutron scattering, nuclear magnetic resonance (NMR), electron spin resonance (ESR), dynamic light scattering (DLS), and optical Kerr effect (OKE) experiments. NMR and ESR experiments have been used extensively to investigate liquid crystals.[31-38] These techniques monitor a single particle correlation time. However, it is necessary to assume the form of the correlation function to interpret the data, and often it is necessary to monitor a probe molecule dissolved in a nematogenic solvent rather than monitoring the nematogen itself. Despite these considerations, NMR and ESR experiments have proven to be extremely valuable tools in the study of liquid crystals.

Dynamic light scattering (DLS)[3] and optical Kerr effect (OKE) experiments give direct access to the orientational correlation function (or its Fourier transform). DLS has been used to measure rotational dynamics in a very wide variety of systems, but in practice it is limited in time resolution. In a DLS experiment, the fast dynamics can appear as a very broad, low-amplitude frequency distribution, making it difficult to observe fast processes in the presence of slower relaxations. A transient grating approach to measure the OKE, first applied by Eyring and Fayer,[39] is the time domain analog of the DLS experiment.[40,41] The time resolution of TG-OKE is limited only by the pulse width of the laser. In the time domain it is possible to separate fast and slow contributions to the signal more readily than in the frequency domain, and the time domain experiments provide increased dynamic range, making it possible to observe the full scope of dynamics in a complex system.

II. Background

A. The TG-OKE Experiment. In the transient grating experiment, two optical pulses are overlapped in time and space, creating an optical interference pattern. The interference pattern, through the OKE, creates a spatially varying orientational anisotropy in the sample. This spatially periodic anisotropy acts as a Bragg diffraction grating. If the pulses are much faster than the material's response, the material reacts with the impulse response function $G(t)$. By diffracting a variably delayed third pulse, the probe, from the grating induced in the sample, the decay of the anisotropy induced by the excitation pulses can be observed. The diffracted intensity is given by

$$I(t) \propto |\chi^{(3)}(t)|^2 \propto |\delta\epsilon(t)|^2 \propto |G^{\epsilon\epsilon}(t)|^2 \qquad (1a)$$

Here $\chi^{(3)}$ is the third-order nonlinear susceptibility, $\delta\epsilon$ is the grating's peak–null difference of the dielectric constant, and $G^{\epsilon\epsilon}$ is the impulse response function of the dielectric tensor.

$$\mathbf{G}^{\epsilon\epsilon}(t) = -\frac{\Theta(t)}{k_B T}\frac{\partial}{\partial t}\mathbf{C}^{\epsilon\epsilon}(t) \qquad (1b)$$

$\Theta(t)$ is a unit step function, and $C^{\epsilon\epsilon}$ is the dielectric time correlation function.

It has been shown by Etchepare[42] and extended by Deeg and Fayer[43] that it is possible to select out specific elements of the $\chi^{(3)}$ tensor by controlling the polarizations of each excitation beam, the probe beam, and polarization of observation of the signal beam. With a macroscopically isotropic sample, it is possible to separate the electronic OKE (instantaneous polarization of the electrons) and the nuclear OKE (orientational anisotropy). Acoustic response of the sample can be eliminated by using a polarization grating.[39,43]

B. Landau–de Gennes Theory. Landau–de Gennes theory as applied to liquid crystals defines the free energy as an expansion in powers of the order parameter. De Gennes extended the Landau theory of the second-order phase transition to the weakly first-order nematic–isotropic phase transition.[44,45] Landau–de Gennes theory provides a good description of the phase transition and the pretransitional region. The free energy expansion is

$$F_n = F_i + \frac{1}{3}a(T - T^*)S_l^2 - \frac{2}{27}BS_l^3 + \frac{1}{9}CS_l^4 \qquad (2)$$

where F_n is the free energy of the nematic phase, F_i is the free energy of the isotropic phase, a, B, C are constants, T^* is a temperature slightly below T_{ni}, and S_l is the order parameter.

In the isotropic phase, just about the phase transition, there are regions of orientationally correlated molecules. In the Landau–de Gennes theory the correlations have an Ornstein–Zernike form[10]

$$\langle S_l(0)\, S_l(R)\rangle \approx (1/R)e^{-R/\xi} \qquad (3)$$

ξ is the correlation length and R is distance. The temperature

dependence of the correlation length is given by[10]

$$\xi = \xi_0\left(\frac{T^*}{T - T^*}\right)^{1/2} \quad (4)$$

De Gennes identifies ξ_0 as a molecular dimension. Works by Courtens,[46,47] Chu et al.,[48,49] and Stinson and Litster[50] have measured ξ_0 and found it to be in the range 5.5–7 Å. This is comparable to the cube root of the molecular volume (~8 Å). For comparison the molecular length of MBBA is 18 Å.

The slow reorientational dynamics of normal liquids can be described by Debye–Stokes–Einstein (DSE) hydrodynamic equation[2,51]

$$\tau = \frac{V_{\text{eff}}\eta(T)}{kT} \quad (5)$$

where V_{eff} is the effective volume of the molecule,[52,53] η is the viscosity, and k is the Boltzmann constant. A modified Debye–Stokes–Einstein equation, according to LdG theory, is used to describe the long time scale reorientational dynamics of pseudonematic domains

$$\tau = \frac{V^*_{\text{eff}}\eta(T)}{k(T - T^*)^\gamma} \quad (6)$$

V^*_{eff} has a somewhat different definition[26,27] than V_{eff} in eq 5. For liquid crystals γ has been shown to be ~1, indicating the validity of the application of mean field theory.[10]

At a high enough temperature one would expect the domain size to be small enough that the isotropic phase of a liquid crystal would behave as a normal liquid. Early measurements of MBBA orientational relaxation were performed over a limited temperature range that did not reach temperatures at which the theory no longer holds.[20,54] Recent measurements over a broad temperature range on MBBA[5b] and on the liquid crystal 5CB[5a] observed the deviations from the LdG theory well above T_{ni}.

C. Ultrafast Dynamics. The dynamics observed with the TG-OKE experiments start with an anisotropy induced in the sample by the excitation beams. The coupling of the radiation field to the molecules involves stimulated Raman scattering exciting librational motions of the molecules.[25,43,55–59] Librations are localized angular vibrations. (The librational motions almost certainly have associated with them a translational displacement of the center of mass. However, with this in mind, we will use the term libration, the conventional terminology.) These motions are modes of the potential surface associated with the fixed local structure of the liquid which exists on the ultrashort time scale of the excitation pulses. Because the pulses are short, they have a broad frequency bandwidth (~100 cm^{-1}). Thus, the pulse contains both frequencies necessary to excite the low-frequency (a few tens of cm^{-1}) librations by stimulated Raman scattering. The orientation of the excited librations is determined by the polarization of the excitation radiation field. Therefore, the laser-excited librations add to the isotropic distribution of thermally excited librations, making the ensemble of excited librations anisotropic. The initial ultrafast transient (~100 fs) seen in TG-OKE experiments consists of a raise in the signal as the overdamped librators begin to undergo angular displacement and the partial decay of the signal as the librational motion dampens.

In a crystal, stimulated Raman scattering excites optical phonons. Because of the well-defined lattice structure, damping of the optical phonons returns the molecules to their original positions, leaving no residual anisotropy. In a liquid, damping of the optically excited librations can leave the molecules orientationally displaced from their initial configurations. This leaves a long-lived residual anisotropy that will eventually decay by some form of orientational relaxation. In a simple liquid, such as biphenyl,[25] one observes the fast librational motions and a biexponential decay of the long-lived residual anisotropy. The anisotropy decays by orientational diffusion, and both components of the biexponential obey the DSE equation.[25] The dynamics observed in the isotropic phase of liquid crystals is fundamentally different because of the strong, anisotropic intermolecular interactions that give rise to local order. Following the ultrafast librational dynamics, there is fast nonexponential orientational relaxation (intradomain dynamics) that is viscosity/temperature independent. On a longer time scale, there is domain randomization. It is the orientational dynamics following the librational damping that will be discussed in detail below. Very general, detailed quantum mechanical descriptions have been given for the relaxation of a thermal excitation of a noncrystalline material that, nonetheless, has local structure. See, for example, Dissado et al.[60] and references therein. Concepts presented in the quantum mechanical treatments apply here as well. However, since the energies of the oscillators are small compared to kT, the dynamics will be discussed classically. Furthermore, the experiments only observe the anisotropy induced by the excitation fields. Therefore, the isotropic background of thermal excitations need not be considered.

III. Experimental Procedures

Two laser systems were used to conduct the experiments: a tunable subpicosecond laser system for the fast dynamics and a ~100-ps Nd:YAG system for the slow (nanosecond) dynamics. The subpicosecond system has been described in detail elsewhere.[61] The 70-ps output pulses of a CW mode-locked Nd:YAG laser at a repetition rate of 83 MHz are sent through an optical pulse compressor and frequency doubled. The resulting 2.5-ps pulses at 532 nm are used to synchronously pump a linear astigmatically compensated three-mirror dye laser that is tuned by a single plate birefringent filter. The dye pulses are amplified by pumping a three-stage amplifier with the frequency-doubled pulses from a cavity dumped, Q-switched and mode-locked Nd:YAG laser operating at a 1.7-kHz repetition rate. The laser system is slightly different from the one described by Newell et al. A 4X telescope has been added to the cavity to increase the spot size at the $LiNbO_3$ crystal, reducing the rate of photorefractive damage. For DCM, typical pulse widths are 200 fs with an average pulse energy of 10–20 μJ. Pulse energies used in the experiments were in the range 200 nJ–1 μJ. An excitation and probe wavelength of 665 nm was employed to avoid two-photon absorption. The amplified pulse is split into three pulses to yield the two excitation pulses and the probe pulse. The two excitation pulses, focused to 120-μm spot sizes, are crossed at an angle of 15° to produce the optical interference pattern, giving rise to the OKE grating. This grating is monitored by the 90-μm spot size probe pulse that is incident at the phase matching angle for Bragg diffraction (slightly noncollinear with the excitation beam to achieve spatial separation). The probe pulse is variably delayed by an optical delay line that is controlled by a 1-μm-resolution stepper motor. This is used for the short time scale measurements. The stepper motor delay line is mounted on a long optical rail and can be moved along the optical rail with a computer-controlled dc motor. This is used for the nanosecond time scale measurements.

The intensity as well as the polarization of all three beams can be independently controlled by half-wave plates and linear polarizers. A fourth linear polarizer is set in the signal path and permits any polarization of the diffracted beam to be monitored. In the measurements made on the femtosecond to a few picoseconds time scale, polarization selective methods were used to independently examine the electronic and nuclear optical Kerr effect. One excitation beam is vertically polarized, one is at 45°, and the probe has horizontal polarization. The signal is detected through the polarizer which is set at 56° (electronic optical Kerr effect) or at 135° (nuclear optical Kerr effect). One of the excitation beams or the probe beam is chopped, and the signal is detected by a photomultiplier tube (PMT). The output of the

PMT is measured by gated integrator and digitized by a computer that also controls the scanning of the optical delay line. To reduce the effects of laser intensity fluctuations, the intensity of the laser is monitored and shots that are outside of a ±10% window are not used. The laser is synchronized to a chopper creating a digital lock-in amplifier. When one of the excitation beams is blocked, the scattered light level is measured. This is normalized to the reference of the adjacent signal shot and is subtracted from the signal shot.

For the slow decay component of the signal, a 100-ps Q-switched and mode-locked YAG was used. The sample is excited with 1.06-μm pulses and probed with a 532-nm pulse. Better signal to noise is achievable with this system for two reasons. The longer pulse creates a larger long time anisotropy, and the use of two colors decreases scattered light problems by permitting scattered excitation light to be filtered out. A polarization grating was used to improve the signal-to-noise ratio and to eliminate acoustic wave generation.[39] One of the IR excitation beams is chopped. The laser is run synchronously with this chopper. The output of the PMT is measured using a lock-in amplifier and digitized and stored on computer. The delay line is also computer controlled, which permits averaging of a number of delay line scans.

The MBBA was obtained from American Tokyo Kassei. The sample was filtered through a 0.2-μm Gelman Acrodisc CR filter. The MBBA was used without further purification. The MBBA was placed in a spectroscopic cell, degassed with several freeze (liquid nitrogen)–thaw cycles on a vacuum line, and sealed under vacuum. The sample was temperature controlled to within 0.1 °C by placing the cell in a temperature-regulated heated aluminum holder. The temperature was measured using a separate platinum resistance thermometer. The phase transition of the MBBA (determined by observing the clearing temperature) is $T_{ni} = 46.9°$. MBBA reacts with water at elevated temperatures. The water adds across the C=N linkage between the two rings in MBBA. This contamination leads to a drop in the clearing temperature. The measurements on MBBA reported in the literature have been on samples of greatly varying clearing temperature, indicating the range of purities used. The high clearing temperature of the samples used in these experiments is indicative of the high purity of the MBBA.

IV. Results

Figure 1 displays TG-OKE data taken on MBBA at 68.3 °C. In panel (a), the electronic optical Kerr effect and the nuclear optical Kerr effect data are shown. The electronic trace is centered at $t = 0$ and gives the instrument response of the experimental apparatus. The nuclear curve (molecular orientational dynamics) shows a small but real displacement from the electronic curve. The very fast rise and decay, out to approximately 1 ps, are caused by the librational dynamics as discussed in section II.C. All of the data sets begin with this very fast feature. The data from 1 to 4 ps are blown up by a factor of 20. After 2 ps the decay is almost flat in this plot. In panel (b), the very fast decay is the continuation of the data that appear flat in panel (a). The data become almost flat after ~100 ps. In panel (c), the steep part of the data at short time is the almost flat data displayed in (b). Clearly, these data are highly nonexponential. It spans a very wide range of time (tens of femtoseconds to tens of nanoseconds) and spans a very broad dynamic range of signal intensity.

The data can be divided into three time ranges. At very short time (<1 ps), the data reflect the librational dynamics discussed briefly in section II.C. The very short time behavior will not be considered further. The intermediate time scale data (~1 ps to ~1 ns) represent the intradomain dynamics, and the long time scale data (>1 ns) result from the randomization of the pseudonematic domains that can be discussed in terms of the LdG theory.

The long time scale dynamics were fit to a squared exponential, since the observable is the square of the response function (see

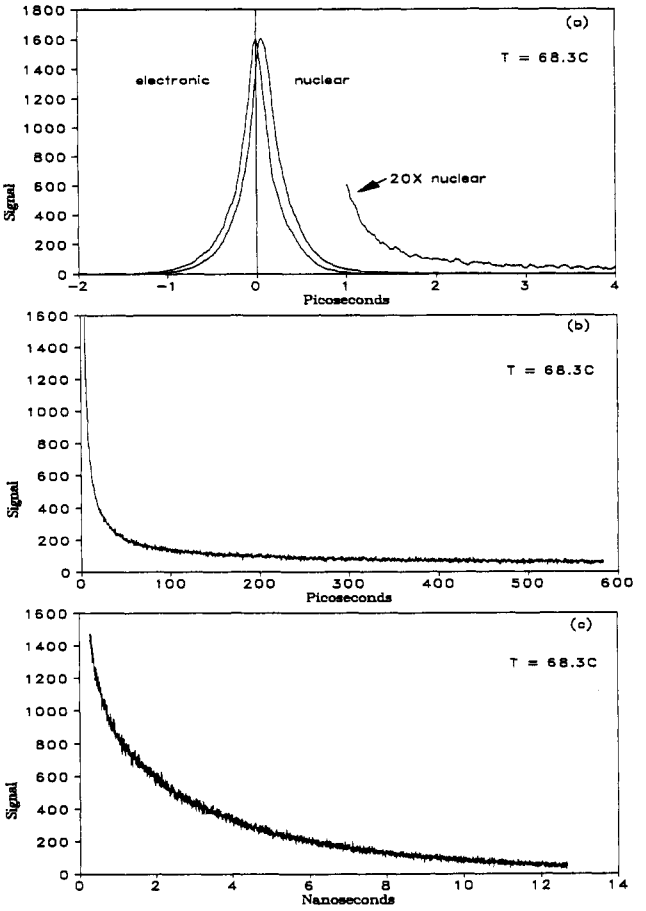

Figure 1. Transient grating optical Kerr effect data for MBBA at 68.3 °C. (a) Electronic and nuclear optical Kerr effect. The electronic effect, centered at $t = 0$, gives the instrument response. The nuclear effect arises from the orientational dynamics of the MBBA. The short time behavior reflects librational dynamics. For $t > \sim 1$ ps the data are multiplied by 20. This is the beginning of the orientational relaxation. (b) The time scale is expanded. The steep part of the decay is the almost flat part (>2 ps) in panel (a). (c) The time scale is expanded. The steep part of the decay is the almost flat part (>30 ps) in (b). The data is nonexponential and spans a very broad range of time scales and a very broad range of signal amplitudes.

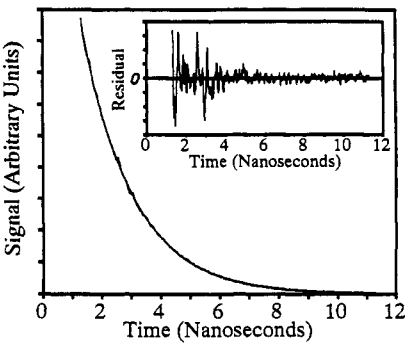

Figure 2. Typical data for the slowest component of the orientational relaxation, which is described by Landau–de Gennes theory. This portion of the data is a single exponential. The data are shown with a single-exponential fit through it, and the inset shows the residuals, greatly magnified.

eq 1).[39-41] To analyze the faster dynamics, the square root of the data was taken to eliminate cross terms in eq 1. The slow LdG exponential decay is subtracted from the full data set, leaving the faster data.

A. Slow Dynamics. The MBBA slow orientational relaxation decay constant was measured as a function of temperature from 49.4 to 119.7 °C. Typical data are shown in Figure 2. The decay time for the pseudonematic domain randomization varies

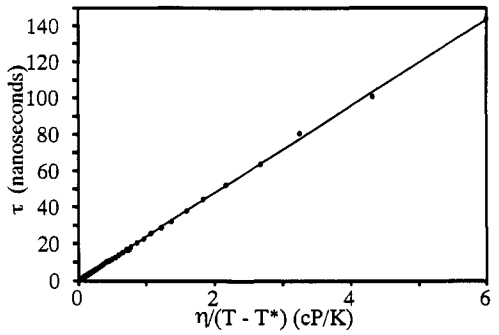

Figure 3. Slowest component decay times vs the viscosity divided by the temperature minus the clearing temperature. The straight line is the fit to the Landau–de Gennes theory over the lower range of temperatures.

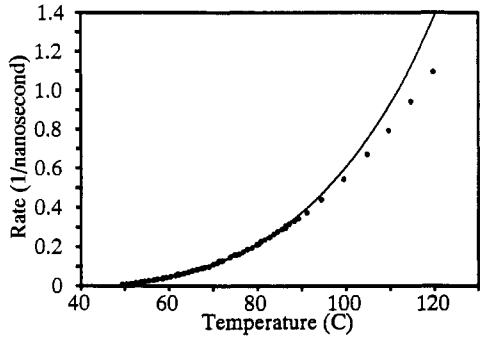

Figure 4. Rate vs temperature for slowest component of the decay. The solid line is the Landau–de Gennes theory curve. Deviation from Landau–de Gennes theory begins at ~90 °C, corresponding to a correlation length of $<3\xi_0$.

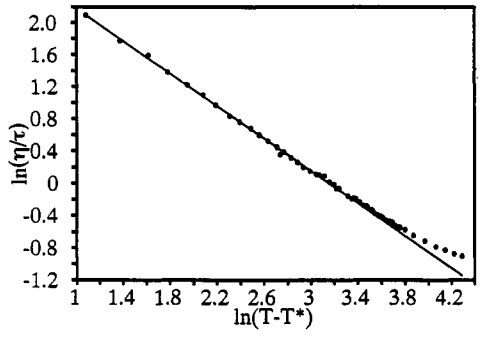

Figure 5. Determination of the exponent γ in eq 6. The value of γ is 1.01 ± 0.01. The deviation at high temperature is due to the inapplicability of the Landau–de Gennes theory when the correlation length falls below $3\xi_0$.

from 174 to 0.91 ns over the temperature range. The decay times vs $\eta/(T - T^*)$ obtained at the lower temperatures and a fit to the LdG theory are shown in Figure 3. The viscosity, η, of MBBA has been reported by Martinoty and Candau.[62] T^* was determined using a formula by de Gennes[10] followed by a slight variation in the fit. T^* was found to be 319.6 K. Since at high enough temperature the data must deviate from the LdG theory, the fit was performed over several low-temperature ranges to assure the theory is applicable. The LdG curve was fit for 49.4 → 60 °C, 49.4 → 70.0 °C, and 49.4 → 80.3 °C. All three fits gave the same slope to within 1%, providing an accurate determination of the LdG curve.

All of the slow data (full temperature range) and the LdG curve obtained from Figure 3 are plotted as rate vs temperature in Figure 4. The fit to the LdG theory is good over a surprisingly wide temperature range with deviation beginning at ~90 °C. At this temperature the correlation length is somewhat less than $3\xi_0$. The data are also plotted as $\ln(\eta/t)$ vs $\ln(T - T^*)$ in Figure 5. At the lower temperatures, the data are clearly fit by a straight line that corresponds to $\gamma = 1$. The deviations at higher temperatures cannot be accounted for by a change in γ. An

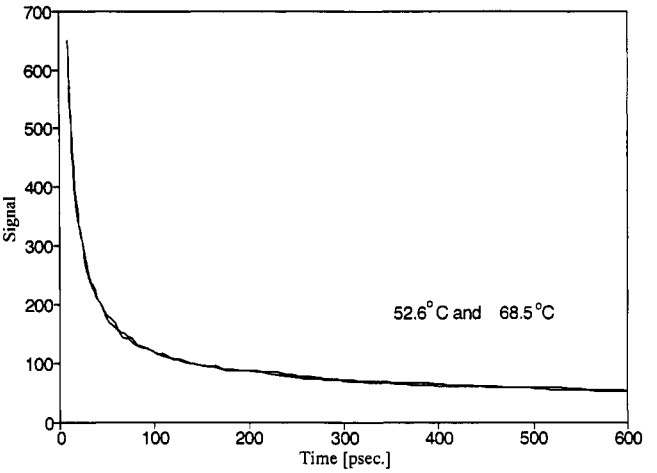

Figure 6. Fast components of decays taken at two temperatures, 52.6 and 68.5 °C. The data are superimposable, showing no viscosity/temperature dependence. The viscosities are 15.8 and 9.3 P at 52.6 and 68.5 °C, respectively.

accurate value of γ was obtained from the fit in Figure 5; γ is 1.01 ± 0.01. Previous light scattering and optical Kerr effect experiments on MBBA covered a narrow temperature range.[20,54] These studies also gave a value of $\gamma = 1$. Because of the large temperature range covered here, to our knowledge this is the most accurate determination of the exponent γ and supports the applicability of mean field theory[10] over a broad range of temperatures.

Deeg et al. also used transient grating experiments to examine the behavior of the liquid crystal 5CB (pentylcyanobiphenyl). The long time portion of the 5CB data was fit to the LdG theory. In 5CB, deviation from the LdG theory also occurred when the correlation length became somewhat less than $3\xi_0$. The range of applicability of the LdG theory was virtually identical for 5CB and MBBA.

When the correlation length in the isotropic phase falls below $3\xi_0$, the liquid crystals begins to make a transition from an ordered liquid to a simple liquid. It is remarkable that the orientational dynamics follow the LdG theory to $\xi \approx 3\xi_0$. This demonstrates the profound effect that local ordering in a liquid can have on liquid-state dynamics.[5] Static variables only display LdG behavior for correlation lengths greater than $4.5–5.5\xi_0$ (10–15 deg above T_c).[22] The transition to a simple liquid will occur over a broad temperature range. If a sufficiently high temperature could be reached, the orientational relaxation should display the normal DSE behavior of a simple liquid. For temperatures at which $\xi < 3\xi_0$ but below the onset temperature for DSE behavior, MBBA and 5CB will display dynamics that do not follow the LdG theory but are, nonetheless, strongly influenced by the details of the local liquid structure. In this range of temperatures, thermal fluctuations are not sufficient to totally overcome intermolecular interactions that affect orientational dynamics. $3\xi_0$ is the minimum correlation length for which the LdG theory applies. Therefore, it can be considered to be the minimum pseudonematic domain size. As mentioned above, ξ_0 for MBBA is between 5.5 and 7 Å.[46–49] This is approximately the length that gives rise to the (spherical) molecular volume. Thus, within $3\xi_0$ there are ~27 molecules. Even using the length for ξ_0 de Gennes used initially,[10] the number of molecules is only ~56.

B. Fast Dynamics. Figure 6 displays the fast, intradomain orientational relaxation dynamics for two temperatures, 52.6 and 68.5 °C. As is clear from the figure, the two data sets are identical in spite of the large change in the viscosity of the sample and the large change in the slow time scale decays over this temperature range. Figure 7a shows a log–log plot of four data sets taken at 52.6, 60.8, 68.5, and 78.2 °C. Within experimental error, all of the data sets display identical highly nonexponential decays. The

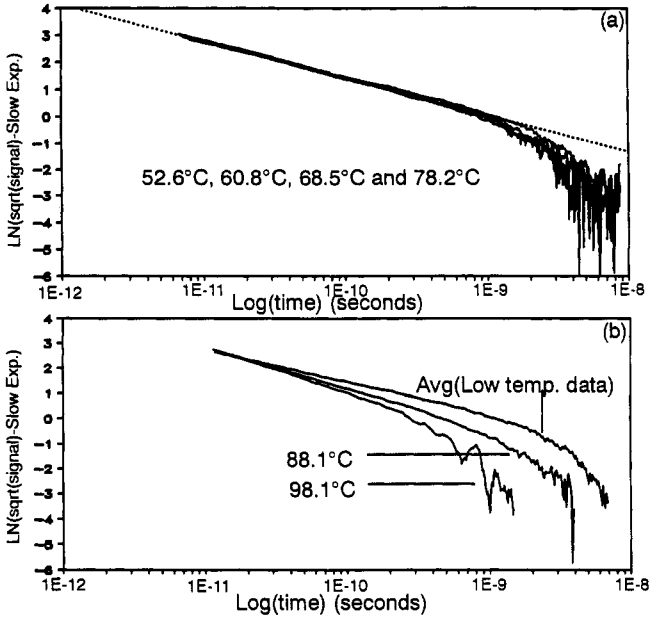

Figure 7. (a) Fast decay data sets at four temperatures (52.6 → 78.2 °C) are plotted vs time on a log–log plot. The decays are superimposable, showing that the fast MBBA dynamics are viscosity/temperature independent. The dotted line is a straight line throught the data showing that the decays obey a power law ($t^{-\alpha}$) with $\alpha = 0.63 \pm 0.03$. (b) The average of the lower temperature data displayed in (a) and two data sets taken at higher temperatures. When the correlation length falls below $3\xi_0$ and the Landau–de Gennes theory no longer describes the slow decay component, the fast dynamics become temperature dependent.

decays are viscosity/temperature independent. Figure 7b compares the average of the lower-temperature decays (all curves from Figure 7a) with higher-temperature decays. The faster dynamics become temperature dependent at ~88.1 °C. This is the same temperature range where the slow dynamics begin to deviate from LdG theory, i.e., the temperature range in which the correlation length becomes so small that pseudonematic domains no longer exist. This behavior is identical to that which was observed previously in 5CB. As long as the correlation length is sufficiently long for pseudonematic domains to exist, as demonstrated by the slow dynamics obeying the LdG theory, the fast intradomain dynamics are viscosity/temperature independent. Thus, the fast, intradomain dynamics are not hydrodynamic, and the results indicate that the dynamics are strongly influenced by the pseudonematic domain structure.

As can be seen in Figure 7a, for times shorter than 1 ns, the data fall on a straight line, corresponding to a power law decay.

$$G(t) = G_0 t^{-\alpha} \tag{7}$$

From the data, α is 0.63 ± 0.03. Figure 8 shows the fast dynamics in 5CB.[5a] These data are also a power law with $\alpha = 0.63 \pm 0.02$. Thus, qualitatively and quantitatively, the orientational relaxation dynamics in the isotropic phase of both liquid crystals, MBBA and 5CB, are strikingly similar. In both systems, the slow dynamics are accurately described by the LdG theory until the correlation length falls just below $3\xi_0$. At higher temperatures, deviation from the LdG theory is observed. The fast intradomain dynamics are viscosity/temperature independent from the nematic–isotropic phase transition to the temperature at which the correlation length falls below $3\xi_0$. When the correlation length becomes less than $3\xi_0$, the fast dynamics become temperature dependent. In the temperature-independent range, the fast dynamics decay as a power law, $t^{-\alpha}$, with α equal to 0.63 for both systems. These identical features of the two systems may suggest that there is universal, fundamental dynamical behavior of the isotropic phase of liquid crystals.

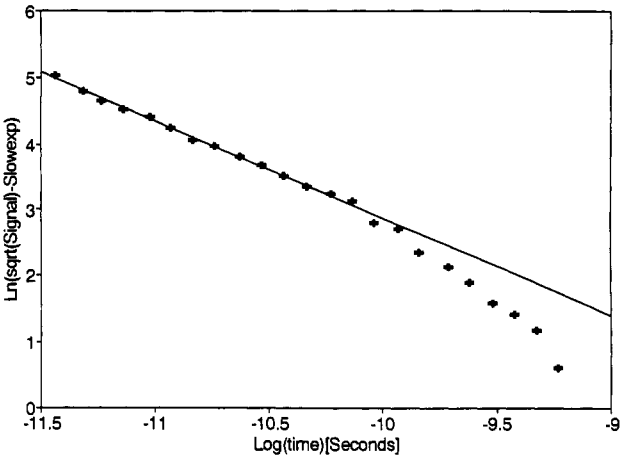

Figure 8. Data taken previously on the liquid crystal 5CB[5] also display a power law decay with the identical exponent, $\alpha = 0.63 \pm 0.02$. The 5CB data are also viscosity/temperature independent until the correlation length falls below $3\xi_0$. The striking similarities in the temperature-dependent dynamics of MBBA and 5CB may indicate a universal behavior in the isotropic phase of liquid crystals.

V. Model for the Temperature-Independent Fast Dynamics

As demonstrated above, MBBA, like 5CB, displays temperature-independent dynamics over broad time range and a sizable temperature span. Recently, several polymers in solutions and melts[8] have been observed to have viscosity/temperature-independent orientational relaxation of side groups on a picosecond time scale. The molecular liquid 2-ethylnaphthalene also displays a fast orientational relaxation component that is viscosity/temperature independent.[6,7] All of these liquids have in common significant local structure caused by either strong anisotropic intermolecular interactions or backbone structure and side group steric interactions. These local structures exist for a time scale long compared to the time scale of the temperature-independent orientational relaxation. The fast dynamics of the two liquid crystals and 2-ethylnaphthalene become temperature dependent at sufficiently high temperatures such that the time scale for slower hydrodynamics processes that destroy the local structures becomes comparable to the that of the fast dynamics. In the polymers studied, the motions of the backbone that will modify the local side group configurations are so slow that the picosecond side group orientational dynamics were not observed to be viscosity/temperature dependent even though η/kT was change by a factor of 30.

The above consideration indicates that local structures are responsible for the temperature-independent dynamics. In the liquid crystals, as long as the pseudonematic local structure lasts for a time longer than the intradomain relaxation, the dynamics are temperature independent. The MBBA sample is isotropic prior to excitation. The order parameter, S, is zero. Application of the E field induces an anisotropy. This is illustrated in Figure 9 for the macroscopic system. The system begins at $S = 0$, the minimum of the free energy surface. When the field is applied, the potential surface shifts; the system wants to align under the influence of the field. During the pulse, the system evolves along the new surface. When the field is removed, the potential returns to the field-free surface. This leaves the system with $S \neq 0$, not at the bottom of the well. Evolution will now occur on the field-free surface to reestablish $S = 0$.

To gain further insight, it is necessary to consider the problem microscopically. There are two contributions to the relaxation illustrated in Figure 9, intradomain and domain randomization. The vast majority of the dynamics is intradomain relaxation. The E field induces a small net alignment of individual molecules. The molecular alignments change the local order parameter, S_l. Unlike S, which is a macroscopic parameter, S_l is nonzero prior to the application of the optical field. S_l defines the local nematic

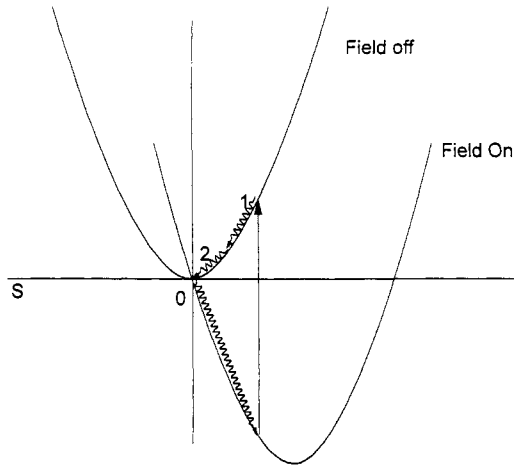

Figure 9. Schematic illustration of the TG-OKE experiment for the macroscopic sample. Initially, the order parameter, $S = 0$, is the minimum of the free energy surface (field off). When the field is applied, the potential surface shifts (field on); the system wants to align under the influence of the field. During the pulse, the system evolves along the new surface. When the field is removed, the potential returns to the field off surface. This leaves the system with $S \neq 0$, not at the bottom of the well. Application of the E field induces an anisotropy. Evolution will now occur on the surface to reestablish $S = 0$. Relaxation of the induced anisotropy has two components: (1) intradomain relaxation giving rise to the fast dynamics and (2) domain randomization giving rise to the slow dynamics as described by Landau–de Gennes theory.

structure relative to the local director associated with a given pseudonematic domain. This is illustrated in cartoon fashion in Figure 10a. (For clarity, the amount of order and the magnitude of the field-induced changes have been exaggerated.) Initially, $S_l = S_l^0$. Immediately following the application of the field, $S_l > S_l^0$. The alignment of the molecules with the field not only increases S_l but also rotates the direction of the local director. Fast intradomain relaxation now occurs, restoring the local order parameter to S_l^0. This results in the decay of most of the signal but leaves the ensemble of domain local directors slightly aligned with the direction defined by the optical field. This long-lived anisotropy can only decay by randomization of the domains and is responsible for the multinanosecond decay described by the LdG theory. Returning to Figure 9, the first part of the relaxation (labeled 1) is intradomain dynamics reestablishing the local order parameters to S_l^0. The final part of the macroscopic relaxation (labeled 2) is domain randomization which finally returns S to a value of zero.

In Figure 10b, the intradomain dynamics are illustrated in terms of the momentary, local free energy surface. Locally the system begins with $S_l = S_l^0$, the minimum of the potential well. This local minimum exists on a time scale short compared to the LdG relaxation time. When the optical field is on, the system evolves microscopically in a manner like that illustrated in Figure 9. Following the optical pulse, the system is left with $S_l \neq S_l^0$. S_l may be larger or smaller than S_l^0, depending on the angle between the applied E field and the original local director. The perturbed local structure is represented by a position on the side of the potential well. This results in a driving force that will cause relaxation of the local structure back to a configuration having $S_l = S_l^0$. Thus, the fast time scale intradomain dynamics are relaxation on a potential surface that returns the domain to the favored local structure, rather than randomization of the local structure.

In this model, a change in temperature changes the viscosity of the liquid, changes the domain size, and changes the time scale of domain randomization. However, as long as the domains exist ($\xi > 3\xi_0$) and the time for domain randomization (time for the loss of the local structure) is long compared to the intradomain relaxation, the fast dynamics will be temperature independent. The local structure is defined by the anisotropic intermolecular interactions which determine the shape of the potential surface. The rate of relaxation is also determined by the shape of the potential surface. If the shape of the momentary, local potential surface is essentially independent of temperature, then the dynamics will also be independent of temperature. It is important to point out that the experiments might not detect a very weak dependence on the absolute temperature. For example, if there is a temperature dependence of $\sqrt{T}$, it is possible that it would not be observed since this would correspond to only a 4% change over the temperature range examined. What is required to observe temperature-independent dynamics is a local potential surface which has a shape independent of temperature or very weakly dependent on temperature.

So far we have discussed two order parameters, S and S_l. S is the macroscopic order parameter. Since we are concerned with the isotropic phase, $S = 0$ expect for a brief time interval following optical excitation when a macroscopic anisotropy has been induced in the sample. S_l is the local order parameter that defines the pseudonematic structure that exists on a distance scale of the correlation length, ξ, for a time short compared to the time scale for domain randomization. We will now define an even smaller distance scale, $\xi_m \ll \xi$, in order to discuss the "microscopic" dynamics in small volumes internal to a pseudonematic domain. On each of these distance scales, we can define the free energy, an order parameter, and a length.

	local	micro
free energy	$F(R,t)$	$f(r,t)$
order parameter	$S_l(R,t)$	$S_m(r,t)$
correlation length	$\xi(T)$	ξ_m

R is a vector giving the location of a domain in the sample, and r is a vector giving the location of a microenvironment inside a particular domain.

The slow dynamics are interpreted in the framework of LdG theory. De Gennes expanded the free energy of a liquid crystalline system in terms of the order parameter S_l (in our notation). When the electric field of the pulse moves the macroscopic system away from $S = 0$, the slow relaxation of the system back to equilibrium (domain randomization) will occur at a rate proportional to the slope of the pseudonematic domain free energy surface. The rate is determined by the domain size, which in turn is determined by the temperature. For time $t > t_0$ which marks the end of the fast intradomain dynamics[10]

$$\frac{\partial S_l(R,t)}{\partial t} = -\frac{1}{\eta}\frac{\partial F(R,t)}{\partial S_l} = -\Gamma(T)\, S_l(R,t) \qquad (8)$$

On the faster time scale, the intradomain dynamics are controlled by the subdomain structure characterized by the parameter S_m. S_m should be thought of as a local structure parameter. An equation analogous to eq 8 may be written for the microenvironment dynamics for time $t < t_0$.

$$\frac{\partial S_m(r,t)}{\partial t} = -\frac{1}{\eta_m}\frac{\partial f(r,t)}{\partial S_m} = -\Gamma_m(r)\, S_m(r,t) \qquad (9)$$

η_m is a microviscosity. Here the rate is a function of the position, r, within the domain, not a function of temperature. There can be a broad distribution of microenvironment structures and, therefore, a broad distribution of $\Gamma_m(r)$. The $\Gamma_m(r)$ become temperature dependent when the domain correlation length is small enough and the domain relaxation time is sufficiently short such that the microenvironment structures are changing on the time scale of $1/\Gamma_m(r)$.

The signal depends only on S, the macroscopic order parameter. As discussed in conjunction with Figures 9 and 10, S reflects the state of S_l. If we consider the S_l's as vectors, then both the lengths and directions are changed by the optical pulse. The fast

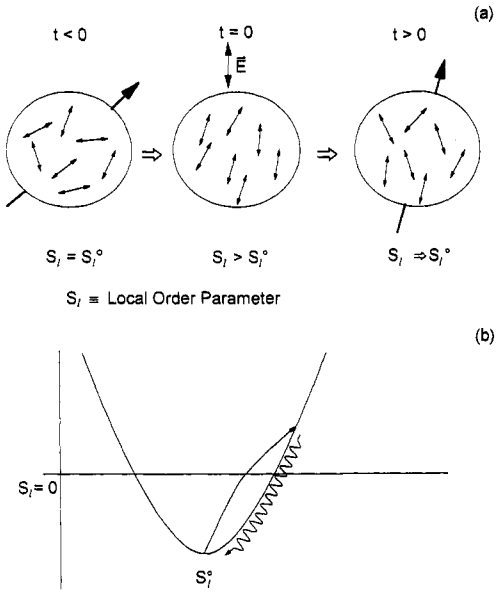

Figure 10. (a) A cartoon of TG-OKE experiment showing the local pseudonematic domain dynamics. For clarity, the amount of order and the magnitude of the field induced changes have been exaggerated. Initially ($t < 0$), $S_l = S_l^0$. Immediately following the application of the field ($t = 0$), $S_l > S_l^0$. The alignment of the molecules with the field not only increases S_l but also rotates the direction of the local director. Fast intradomain relaxation restores the local order parameter to S_l^0. This results in the decay of most of the signal but leaves the ensemble of domain local directors slightly aligned with the direction defined by the optical field. This long-lived anisotropy can only decay by the slow randomization of the domains. (b) Intradomain dynamics are illustrated in terms of the momentary, local free energy surface. Locally the system begins with $S_l = S_l^0$, the minimum of the potential well. This local minimum exists on a time scale short compared to the domain randomization time. Following the optical pulse, the system is left with $S_l \neq S_l^0$. The perturbed local structure is represented by a position on the side of the potential well. This results in a driving force that will cause relaxation back to a configuration having $S_l = S_l^0$. The fast time scale intradomain dynamics are relaxation on a potential surface that returns the domain to the desired local structure, rather than randomization of the local structure.

intradomain dynamics restore the lengths of the vectors. The residual directional anisotropy is relaxed by slow domain randomization. Since the domains are made up of microenvironments, it should be possible to connect the microscopic variables to the macroscopic observables. It can be envisioned that the pseudonematic domain order parameter involves an average over the microenvironment structures.

$$S_l(R,t) = \langle S_m(r,t) \rangle_\xi \tag{10}$$

The average over r is carried out on a distance scale ξ. Making this connection, we can describe the impulse response function of the dielectric tensor (see eq 1). For $t > t_0$

$$G(t) \propto S_l(t) \propto e^{-\Gamma(T)t} \tag{11}$$

This is the hydrodynamic regime described by LdG theory which gives $\Gamma(T)$. For $t < t_0$,

$$G(t) \propto S_l(t) \propto \langle S_m(r,t) \rangle_\xi \propto \sum_i P_i(\Gamma^i_m) e^{-\Gamma^i_m t} \tag{12}$$

Γ^i_m is the rate constant for the relaxation of microenvironments belonging to the ith subensemble of microenvironments. All members of a subensemble have the same relaxation rate. $P_i(\Gamma^i_m)$ is the probability that a microenvironment has the relaxation rate Γ^i_m. The relaxation of the individual microenvironments is taken to be exponential, but there can be a broad distribution of rates. This is discussed further below. Equation 12 describes the nonhydrodynamic regime of temperature-independent fast intradomain relaxation.

The experimental data give the response function (following the librational dynamics) of the form

$$G(t) = G_S(t) + G_f(t) = Ae^{-\Gamma(T)t} + Bt^{-\alpha} \tag{13}$$

where G_S is the response function for the slow dynamics and G_f is the response function for the fast dynamics. The temperature-dependent decay rate for the slow dynamics, $\Gamma(T)$, is described by LdG theory. The power law term must arise from eq 12. There are many physical mechanisms that can give rise to a power law decay. Here we will consider two that seem relevant to the pseudonematic domains of the isotropic phase of liquid crystals. They are a parallel process (Förster direct transfer model) and a serial process (hierarchically constrained dynamics model).

The Parallel Process Model. The microscopic structure parameter, S_m, associated with each microenvironment is altered by the optical field. The relaxation dynamics are characterized by the time evolution of S_m and are determined by slope of the microenvironment free energy surface, $f(S_m)$. Then

$$\frac{\partial S_m}{\partial t} = -\gamma \frac{\partial f(S_m)}{\partial S_m} \tag{14}$$

For a parabolic surface, the time evolution of S_m is exponential with a decay constant, Γ^i_m, as in eq 12. A distribution of curvatures of the parabolic surfaces gives rise to a distribution of Γ^i_m's. Converting the sum in eq 12 into an integral, the observed power law decay will occur if

$$P(\Gamma_m) = \Gamma_m^{\alpha-1} \tag{15}$$

i.e.

$$G_f(t) = \int_{\Gamma_{min}}^{\Gamma_{max}} \Gamma_m^{\alpha-1} e^{-\Gamma_m t} \, d\Gamma_m = \beta t^{-\alpha} \tag{16}$$

where β is a constant. If the limits of integration are 0 to ∞, the decay is a power law over all time. Since a power law is observed over a limited range of times, Γ_{min} and Γ_{max} are finite. To reproduce the observed data, the range of Γ's corresponds to a distribution of parabola constants spanning 2.5 orders of magnitude. The experiments on MBBA and 5CB give $\alpha = 0.63$. Therefore, the probability distribution of relaxation rates is $P(\Gamma_m) = \Gamma_m^{-0.37}$. Similar distributions are seen in other condensed-matter systems. For example, in low-temperature glasses, relaxation rates of glassy two-level systems have been observed to have a distribution[63,64] $P(\Gamma) = \Gamma^{-1}$.

The Serial Process Model. In the parallel process model, each microenvironment relaxes exponentially with a well-defined rate constant. The power law is obtained because of the form of the distribution of relaxation rates in different microenvironments. In the serial process model, which involves constraint release, the dynamics of a microenvironment are not exponential. In the constraint release picture, some degrees of freedom are suppressed unless other degrees of freedom are in particular states.[65,66] Fast dynamics on a short distance scale bring the system into a configuration that permits somewhat slower dynamics on a longer distance scale, which in turn release constraints that permit even slower dynamics on an even longer distance scale. This occurs until the longest distance scale is reached with a corresponding longest time scale dynamics. Here, the longest distance scale is ξ_m, the correlation length of the microenvironment, and the longest time scale is associated with a time, τ_{max}.

The hierarchically constrained dynamics model[65] has been applied to relaxation of glassy systems. This model will give a stretched exponential decay or a power law decay depending on the distribution of states and the conditions for release of the constraint to allow the next set of motions. Over a wide time range, the constraints can dominate the relaxation dynamics. Palmer et al.[65] demonstrated a model of this type for a distinct series of levels of Ising spins. Here we will use the results of this

model to discuss relaxation dynamics of a microenvironment. For a series of n levels with N_n degrees of freedom in a given level, a constraint is placed on the system such that a relaxation process in the succeeding level $(n+1)$ may not occur unless μ_n elements have relaxed in the previous level (n). By restricting each degree of freedom to have only two states (Ising spin model), one obtains the relationship between the relaxation times of the different levels.

$$\tau_{n+1} = 2^{\mu_n}\tau_n \tag{17}$$

Then the fast intradomain relaxation, $G_f(t)$, is determined by the constraint release dynamics, i.e.

$$G_f(t) = \sum_{n=0}^{\infty} w_n \exp(-t/\tau_n) \tag{18}$$

where $w_n = N_n/N$. w_n is the weight of the decay with decay constant τ_n in the distribution of decays. N_n is the number of states in the nth level; N is the total number of states.

A power law decay, as observed in the experiments, will only occur for certain conditions on μ_n and w_n. The weighting is geometric, with $N_{n+1} = N_n/\lambda$, where $\lambda > 1$. This decreasing weighting allows $N = \sum_{n=0}^{\infty} N_n$ to be convergent. If the number of elements that must relax in each level is the same for all levels, $\mu_n = \mu_0$, τ_{max} is not finite. Since we observe a slowest decay in the power law $G_f(t)$, we require τ_{max} to be finite. Assuming an exponential distribution of the number of elements that must be relaxed to release constraints, $\mu_n = \mu_0 \exp(-\gamma n)$, gives a large but finite τ_{max} for $\gamma \ll 1$. Using these conditions, $G_f(t)$ is a power law for $t < \tau_{max}$,

$$G_f(t) = \beta t^{-(\ln\lambda)/\gamma} = \beta t^{-\alpha} \tag{19a}$$

and a single exponential for $t \gg \tau_{max}$,

$$G_f(t) \propto \exp(-t/\tau_{max}) \tag{19b}$$

Experimentally, $\ln\lambda/\gamma = 0.63$. Since $\gamma \ll 1$, $\lambda \cong 1$. This implies that there are many levels, and the number of states per level falls off very slowly with increasing n. The levels and the states are associated with the structure of the microenvironment. The dynamics will be (essentially) temperature independent until the size of the pseudonematic domain is reduced to the maximum distance scale over which the constraints operate. Therefore, $\xi_m \cong 3\xi_0$ since this is the correlation length for both MBBA and 5CB at which the onset of temperature dependence of the fast dynamics is observed. This corresponds to a length of $\approx$20 Å.

The above discussions show that either a parallel or a serial relaxation model can account for the observed power law decay. However, experiments on other types of systems provide some support for the parallel dynamics. Temperature-independent orientational relaxation has been observed using TG-OKE experiments in several other samples that have significant local structure. These are the pure liquid 2-ethylnaphthalene,[6,7] the side group motions of poly(2-vinylnaphthalene) in solution,[8a] and poly(methylphenylsiloxane) both in the pure polymer melt and in solution.[8b] In these systems, the temperature-independent decays are a single exponential, a biexponential, and a triexponential, respectively. For example, in 2-ethylnaphthalene, there is a temperature-independent decay of 3.5 ps. On a longer time scale there are additional decays that are hydrodynamic and obey the DSE equation. From neutron scattering it is known that naphthalene liquid exists with the naphthalenes in crooked T-shaped local structures that exist for a time short compared to the orientational diffusion time. The fast, temperature-independent decay observe in 2-ethylnaphthalene is attributed to the optical perturbation of the T-shaped structures and then the relaxation on the local potential surface to restore the T. This is the same picture as the parallel process for the liquid crystals except that the liquid crystals have a broad distribution of potential surfaces because of structural inhomogeneity of the microenvironments. This gives the broad distribution of rates and, therefore, the power law. The single temperature-independent exponential observed for 2-ethylnaphthalene cannot be explained in terms of constraint release. In the polymer systems, the local structural relaxations that gives rise to the temperature-independent exponential decays occur on potential surfaces that arise from the backbone geometry and the steric interactions of the side groups. On the short time scale of the local relaxation, the geometry and therefore the potential surfaces are fixed. Thus, the dynamics of all of the systems can be explained as relaxation on parabolic surfaces associated with the local structures that exist for a time scale longer than the relaxation. If the constraint release model is invoked to explain the liquid crystal data, then data for the various samples, which are qualitatively the same, must be described using entirely different models. While this is possible, an appeal to simplicity suggests that the same basic physical phenomena are occurring in all samples.

VI. Concluding Remarks

We have measured the orientation dynamics in the isotropic phase of the liquid crystal MBBA over a wide temperature range and over a very broad range of times (100 fs to 100 ns). The most remarkable observations are the complete lack of temperature dependence of the fast (1 ps < t < 1 ns) orientational dynamics over a range of temperatures in which the viscosity undergoes a large change and the slow dynamics change decay rates by well over an order of magnitude. The temperature-independent fast dynamics are associated with molecular motions in the pseudonematic domains that exist in the isotropic phase near the nematic phase transition. The fast dynamics remain temperature independent until the domain correlation length falls slightly below $3\xi_0$, the same correlation length (and temperature) at which the Landau–de Gennes theory ceases to hold for the slower dynamics.

The MBBA results and TG-OKE measurements on the liquid crystal, 5CB, are remarkably similar. The slow dynamics exhibited by both systems obey the Landau–de Gennes theory over a wide range of temperatures. The slow dynamics involve the orientational randomization of the domains. Deviation from the LdG theory begins when the correlation length becomes slightly less than $3\xi_0$. Within experimental error, the deviation begins at the identical correlation length for the two samples. This may suggest a fundamental minimum correlation length for the existence of local nematic behavior in the isotropic phase. Both MBBA and 5CB exhibit a power law decay, $t^{-\alpha}$, for the fast dynamics. It is remarkable that in both samples α is measured to be 0.63.

The lack of temperature dependence of the fast dynamics is discussed in terms of the local pseudonematic structure that exists in the domains. The onset of temperature dependence coincides with the correlation length becoming so small that the domains cease to exist. The radiation field (or a thermal fluctuation) changes the local order parameter associated with a domain. This moves the system away from the minimum of the local free energy surface that exists on a time scale short compared to the domain randomization time. The system then relaxes back to the minimum. An increase in temperature reduces the domain size. However, as long as it is sufficiently large ($>3\xi_0$), there is a well-defined local structure and a well-defined free energy surface. Since the relaxation dynamics depend on the form of the potential, the dynamics are temperature independent until a temperature is reached at which the time scale for domain randomization is equal to the time scale for intradomain structural relaxation.

MBBA and 5CB show virtually identical temperature-independent fast orientational relaxation dynamics. Several other liquid-state systems have recently been observed to display fast orientation dynamics that are temperature independent.[6-9] All of these system have in common well-defined local structures.

When these structures are perturbed, they relax to the local potential minimum and re-form the local structure. On longer time scales than the relaxation, hydrodynamic randomization occurs. The temperature-independent relaxation should be common to many structured liquids and other molecular materials.

Acknowledgment. This work was supported by the National Science Foundation Division of Materials Research (DMR90-22675).

References and Notes

(1) Debye, P. *Polar Molecules*; Dover: New York, 1929.
(2) Kivelson, D. In *Rotational Dynamics of Small and Macromolecules*; Dorfmüller, T., Pecora, R., Eds.; Springer: Berlin, 1987.
(3) Berne, B. J.; Pecora, R. *Dynamic Light Scattering*; Wiley: New York, 1976.
(4) Misawa, M.; Fukunaga, T. *J. Chem. Phys.* **1990**, *93*, 3495.
(5) (a) Deeg, F. W.; Greenfield, S. R.; Stankus, J. J.; Newell, V. J.; Fayer, M. D. *J. Chem. Phys.* **1990**, *93*, 3503. (b) Stankus, J. J.; Torre, R.; Marshall, C. D.; Greenfield, S. R.; Sengupta, A.; Tokmakoff, A.; Fayer, M. D. *Chem. Phys. Lett.* **1992**, *194*, 213.
(6) Greenfield, S. R.; Sengupta, A.; Stankus, J. J.; Fayer, M. D. *Chem. Phys. Lett.* **1992**, *193*, 49.
(7) Greenfield, S. R.; Stankus, J. J.; Sengupta, A.; Terazima, M.; Fayer, M. D. *J. Phys. Chem.*, in press.
(8) (a) Sengupta, A.; Terazima, M.; Fayer, M. D. *J. Phys. Chem.* **1992**, *96*, 8619. (b) Sengupta, A.; Fayer, M. D. *J. Chem. Phys.*, in press.
(9) Steffen, W.; Patkowski, A.; Meier, G.; Fischer, E. W. *J. Chem. Phys.* **1992**, *96*, 4171.
(10) de Gennes, P. G. *The Physics of Liquid Crystals*; Clarendon: Oxford, 1974.
(11) de Gennes, P. G. *Phys. Lett. A* **1969**, *30*, 454.
(12) Stinson III, T. W.; Litster, J. D. *Phys. Rev. Lett.* **1970**, *25*, 503.
(13) Filippini, J. C.; Poggi, Y. *J. Phys. Lett. (Paris)* **1974**, *35*, L-99.
(14) Coles, H. J. *Mol. Cryst. Liq. Cryst., Lett. Sect.* **1978**, *49*, 67.
(15) Litster, J. D.; Stinson III, T. W. *J. Appl. Phys.* **1970**, *41*, 996.
(16) Cabane, B.; Clarke, G. *Phys. Rev. Lett.* **1970**, *25*, 91.
(17) Gosh, S.; Tettamanti, E.; Indovina, E. *Phys. Rev. Lett.* **1973**, *29*, 638.
(18) Wong, G. K. L.; Shen, Y. R. *Phys. Rev. Lett.* **1973**, *30*, 895.
(19) Wong, G. K. L.; Shen, Y. R. *Phys. Rev. Lett.* **1974**, *32*, 527.
(20) Wong, G. K. L.; Shen, Y. R. *Phys. Rev. A* **1974**, *10*, 1277.
(21) Hanson, E. G.; Shen, Y. R.; Wong, G. K. L. *Phys. Rev. A* **1976**, *14*, 1281.
(22) Filippini, J. C.; Poggi, Y. *J. Phys. Lett. (Paris)* **1976**, *37*, L-17.
(23) Alms, G. R.; Bauer, D. R.; Brauman, J. I.; Pecora, R. J. *Chem. Phys.* **1973**, *58*, 5570.
(24) Alms, G. R.; Bauer, D. R.; Brauman, J. I.; Pecora, R. *J. Chem. Phys.* **1973**, *59*, 5310.
(25) Deeg, F. W.; Stankus, J. J.; Greenfield, S. R.; Newell, V. J.; Fayer, M. D. *J. Chem. Phys.* **1989**, *90*, 6893.
(26) Gierke, T. D.; Flygare, W. H. *J. Chem. Phys.* **1974**, *61*, 2231.
(27) Alms, G. R.; Gierke, T. D.; Flygare, W. H. *J. Chem. Phys.* **1974**, *61*, 4083.
(28) Flytzanis, C.; Shen, Y. R. *Phys. Rev. Lett.* **1974**, *33*, 14.
(29) Lalanne, J. R.; Martin, B.; Pouligny, B.; Kielich, S. *Opt. Commun.* **1976**, *19*, 440.
(30) Amer, N. M.; Lin, Y. S.; Shen, Y. R. *Solid State Commun.* **1975**, *16*, 1157.
(31) *NMR in Liquid Crystals*; Emsley, J. W., Veracini, C. A., Eds.; Reidel: Dordrecht, 1985.
(32) Freed, J. H. In *Rotational Dynamics of Small and Macromolecules*; Dorfmüller, T., Pecora, R., Eds.; Springer: Berlin, 1987.
(33) Beckmann, P. A.; Emsley, J. W.; Luckhurst, G. R.; Turner, D. L. *Mol. Phys.* **1986**, *59*, 97.
(34) Dong, R. Y.; Richards, G. M. *J. Chem. Phys.* **1989**, *91*, 7276.
(35) Poupko, R.; Vold, R. L.; Vold, R. R. *J. Phys. Chem.* **1980**, *84*, 3444.
(36) Selwyn, L. S.; Vold, R. L.; Vold, R. R. *Mol. Phys.* **1985**, *55*, 287.
(37) Polnaszek, C. F.; Freed, J. H. *J. Phys. Chem.* **1975**, *79*, 2287.
(38) Barbara, T. M.; Vold, R. R.; Vold, R. L.; Neubert, M. E. *J. Chem. Phys.* **1985**, *82*, 1612.
(39) Eyring, G.; Fayer, M. D. *J. Chem. Phys.* **1984**, *81*, 4314.
(40) Yan, Y.; Nelson, K. A. *J. Chem. Phys.* **1987**, *87*, 6240.
(41) Yan, Y.; Nelson, K. A. *J. Chem. Phys.* **1987**, *87*, 6257.
(42) Etchepare, J.; Grillon, G.; Chambaret, J. P.; Hamoniaux, G.; Orszag, A. *Opt. Commun.* **1987**, *63*, 329.
(43) Deeg, F. W.; Fayer, M. D. *J. Chem. Phys.* **1989**, *91*, 2269.
(44) de Gennes, P. G. *Mol. Cryst. Liq. Cryst.* **1971**, *12*, 193.
(45) Vertogen, G.; de Jeu, W. H. *Thermotropic Liquid Crystals, Fundamentals*; Springer-Verlag: Berlin, 1988.
(46) Courtens, E.; Koren, G. *Phys. Rev. Lett.* **1975**, *35*, 1711.
(47) Courtens, E. *J. Chem. Phys.* **1977**, *66*, 3995.
(48) Chu, B.; Bak, C. S.; Lin, F. L. *Phys. Rev. Lett.* **1972**, *28*, 1111.
(49) Gulari, E.; Chu, B. *J. Chem. Phys.* **1975**, *62*, 798.
(50) Stinson, T. W.; Litster, J. D. *Phys. Rev. Lett.* **1973**, *30*, 688.
(51) Kivelson, D.; Madden, P. A. *Annu. Rev. Phys. Chem.* **1980**, *31*, 523.
(52) Perrin, F. *J. Phys. Radium* **1934**, *5*, 497.
(53) Hu, C.; Zwanzig, R. *J. Chem. Phys.* **1974**, *60*, 4354.
(54) Prost, J.; Lalanne, J. R. *Phys. Rev. A* **1973**, *8*, 2090.
(55) Ruhman, S.; Nelson, K. A. *J. Chem. Phys.* **1991**, *94*, 859.
(56) Ruhman, S.; Williams, L. R.; Joly, A. G.; Kohler, B.; Nelson, K. A. *J. Phys. Chem.* **1987**, *91*, 2237.
(57) McMorrow, D.; Lotshaw, W. T.; Kenney-Wallace, G. A. *IEEE J. Quantum Electron.* **1988**, *QE-24*, 443.
(58) McMorrow, D.; Lotshaw, W. T.; Kenney-Wallace, G. *Chem. Phys. Lett.* **1988**, *145*, 309.
(59) Deeg, F. W.; Fayer, M. D. *J. Mol. Liq.* **1990**, *45*, 19.
(60) Dissado, L. A.; Nigmatullin, R. R.; Hill, R. M. *Adv. Chem. Phys.* **1985**, *63*, 253.
(61) Newell, V. J.; Deeg, F. W.; Greenfield, S. R.; Fayer, M. D. *J. Opt. Soc. Am. B* **1989**, *6*, 257.
(62) Martinoty, P.; Candau, S.; Debeauvais, F. *Phys. Rev. Lett.* **1971**, *27*, 1123.
(63) Littau, K. A.; Dugan, M. A.; Chen, S.; Fayer, M. D. *J. Chem. Phys.* **1992**, *96*, 3484.
(64) Littau, K. A.; Fayer, M. D. *Chem. Phys. Lett.* **1991**, *176*, 551.
(65) Palmer, R. G.; Stein, D. L.; Abrahams, E.; Anderson, P. W. *Phys. Rev. Lett.* **1984**, *53*, 958.
(66) Ajay; Palmer, R. G. *J. Phys. A: Math. Gen.* **1990**, *23*, 2139.